

Investigation of CsPbBr₃: DC Electrical Properties, Complex Impedance Study, and Optoelectronic Behavior

Hiral Patel^{1*}, Piyush Vyas²

^{1*}Chemistry Department, Amity University, Gwalior-474005, Madhya Pradesh, India,
E-mail: hiralpatela16@gmail.com

²Chemistry Division, Sheth M. N. Science College, Patan-384265, Gujarat, India

ABSTRACT

CsPbBr₃ perovskite was investigated for its structural, optical, electrical, dielectric, and optoelectronic properties. X-ray diffraction confirmed the orthorhombic crystal structure, while FESEM analysis revealed well-defined cubic microstructures. ED-XRF measurements verified the presence of Cs, Pb, and Br elements. Optical studies showed a direct band gap of 2.19 eV and a strong photoluminescence emission at 554 nm. Dielectric properties exhibited frequency- and temperature-dependent behavior, with AC conductivity following Jonscher's power law and DC conductivity obeying Arrhenius behavior with an activation energy of 0.517 eV. Impedance analysis confirmed semiconducting characteristics through negative temperature coefficient resistance (NTCR) behavior. Under 100 mW cm⁻² illumination, the material demonstrated a tenfold increase in photocurrent, with responsivity and detectivity reaching 1.73 mA W⁻¹ and 3.27 × 10⁴ Jones, respectively. Furthermore, reduced grain and grain-boundary resistance under illumination indicated enhanced charge-carrier transport. These results highlight the potential of CsPbBr₃ as a promising material for photodetectors and other optoelectronic applications.

Keywords: CsPbBr₃, perovskite, dielectric properties, impedance spectroscopy, optoelectronic properties, photo detector.

Introduction

This research focuses on CsPbBr₃ perovskite, a material with superior electrical, dielectric, and optoelectronic properties. The research focuses on its microstructure, impedance properties, and photo response with a view to understanding how it would be applicable in photo detectors, solar cells, and LEDs.¹⁻⁴

Perovskite materials, and specifically CsPbBr₃, have received considerable research interest owing to their high dielectric constant, tunable band gap, and improved stability over other conventional organic-inorganic perovskite. Their orthorhombic phase structure is significant in determining their properties in charge transport and in how they absorb light, and they are compatible with next-generation optoelectronic devices.^{5,6} In spite of their potential, nevertheless, more research is needed to understand how external conditions, i.e., temperature and light intensity, influence their electrical and optical properties. By addressing these gaps in knowledge, in this study, we aim to drive the utility and performance improvement of CsPbBr₃-based devices.⁷⁻¹¹

Therefore, the present work focuses on the synthesis and comprehensive characterization of CsPbBr₃ perovskite.¹² Structural analysis is carried out using X-ray diffraction (XRD), while field emission scanning electron microscopy (FESEM) is employed to investigate the surface morphology and microstructure. Elemental composition is examined through energy-dispersive X-ray fluorescence (ED-XRF) spectroscopy.¹³⁻¹⁷ Optical properties are analyzed using UV-Visible absorption and photoluminescence spectroscopy. The dielectric, electrical, and impedance characteristics are studied as functions of frequency and temperature to understand the conduction and relaxation mechanisms. Furthermore, photoresponse measurements are performed under different illumination conditions to evaluate the photodetection capability of the material.¹⁸⁻²¹ The obtained results provide valuable insights into the charge transport dynamics, dielectric behavior, and optoelectronic performance of CsPbBr₃, highlighting its potential for future applications in photodetectors, solar cells, LEDs, and other advanced semiconductor devices.²²⁻²⁵

2. Experimental

The synthesis of CsPbBr₃ was carried out via a solution-based method, ensuring phase purity. Structural analysis was performed using XRD, followed by morphological characterization via FESEM. Elemental composition was verified using ED-XRF spectroscopy. Optical properties were studied using UV-Vis spectroscopy and photoluminescence (PL) measurements. Dielectric behavior was analyzed through impedance spectroscopy across different temperatures and frequencies. Finally, the optoelectronic properties were evaluated using a two-probe method under varying light intensities.

Synthesis of Cesiumleadbromide (CsPbBr₃)

CsPbBr₃ has been synthesized by reacting equimolar amount of cesiumbromide (CsBr) and leadbromide (PbBr₂) at room temperature in ambient environment. In a typical synthesis, 3 mM of CsBr was dissolved in 1.5 mM de-ionized water by ultrasaniation for 2 hour. Hence, 3 mM of PbBr₂ was add with 4.5 ml of aqueous hydrobromicacid (HBr) top repare PbBr₂ precursor. Top recipitate CsPbBr₃, aqueous CsBr was quickly mixed with PbBr₂ precursor and orangecol or CsPbBr₃ was collected by filtration very carefully. Thenas-synthesized material was washed seve raltimes with ethanol and collected by centrifugations. Finally, the sample was dried overnight in vacuum top repare powder sample for further characterizations.

3. Results and Discussion

The XRD pattern of the as-synthesized CsPbBr₃ confirms the formation of a single-phase orthorhombic crystal structure (JCPDS No. 74-2251) with the Pbnm space group. The observed diffraction peaks match the characteristic planes of orthorhombic CsPbBr₃. The calculated Goldschmidt tolerance factor ($t = 0.939$) indicates a stable perovskite lattice with slight distortion from the ideal structure, which can significantly influence its optical and electronic properties. Rietveld refinement using the MAUD software further validates the structural parameters and phase purity of the synthesized sample (Figure 1a). The morphological properties of the as-synthesized CsPbBr₃ powder were investigated using field-emission scanning electron microscopy (FESEM). The FESEM images (Figure 1b) confirm the successful formation of predominantly cubic-shaped particles, which is consistent with the crystal structure of CsPbBr₃. Most particles exhibit well-defined cubic morphology, while a few slightly deformed particles with comparatively smaller dimensions are also observed. A magnified image of a representative particle (Figure 1c) shows a cube with an edge length of approximately 3 μm . The nearly equal edge lengths in all directions indicate isotropic crystal growth, suggesting that the growth rate was almost uniform along different crystallographic orientations. This uniform growth behavior contributed to the formation of well-faceted cubic crystals.

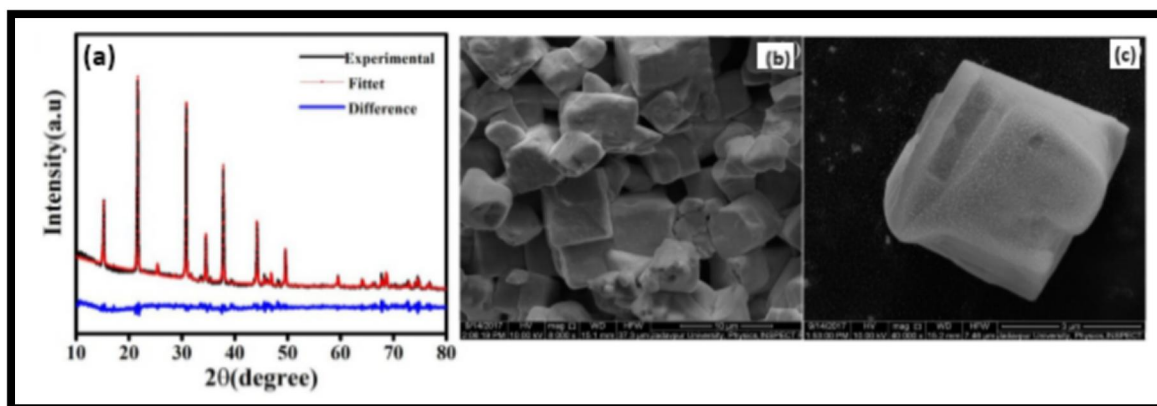


Figure 1: (a) XRD spectra with Rietveld refinement; (b) Cluster of CsPbBr₃ micro cube, (c) Single micro structure of CsPbBr₃

Optical Properties

Absorbance spectra of the sample have been collected in the wavelength range of 300 nm to 800 nm. It is well known that CsPbBr₃ has a direct band gap, which is measured by using Tauc plot. It can be expressed as,

$$\alpha h\nu = (h\nu - E_g)^n$$

Where, α is absorption coefficient, $h\nu$ represents the energy of the incident photon, E_g is the band gap of respective material and $n=1/2$ or 2 for direct and indirect band gap type material. Here $(\alpha h\nu)^2$ vs $h\nu$ has been plotted to calculate the band gap from the interpolation as depicted in (Figure 2a). The band gap of CsPbBr₃ has been appeared as 2.19eV. (Figure 2b) illustrates the PL emission spectra of the powder sample which is excited at 428 nm. It is evident from the figure that a sharp peak has appeared at 554 nm (2.23eV) which may be a rising from band-to-band transition. Over all emission line width is very broad due to the formation of self-trapped excitons instead of dissociation and collection of excitons within material.

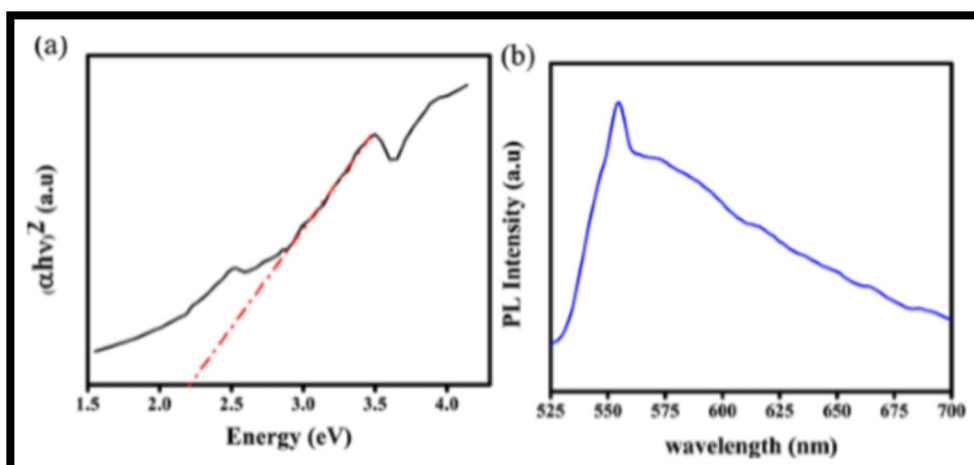


Figure 2: (a) Taucplot (from Uv-Vis spectra) CsPbBr₃; (b) PL spectra of CsPbBr₃

Optoelectronic Properties

To illustrate the photo response capability of CsPbBr₃, two probe method has been used for measuring the I-V profile under simulated solar spectrum of different intensity. (Figure 3a) represents the I-V curves of the photo-detector under light illumination ranging from 0 mW cm⁻²-100 mW cm⁻². The I-V curves maintain a non- linear proportionality with applied bias indicating non-Ohmic type of contact between ITO and CsPbBr₃. As shown in (Figure 3b), photo current increases up to 10 times compared to dark current at light intensity 100 mW cm⁻². The variation of photo current

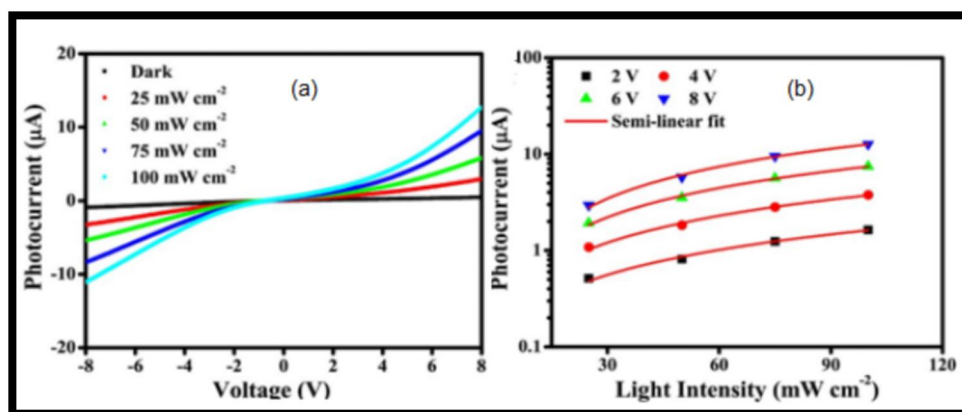


Figure 3: (a) I-V response of the detector; (b) Light dependent photo-current

With light intensity for several applied bias has depicted in (Figure 3b). The light dependence of current can be expressed as $I_{ph} \sim P^\alpha$, where α signifies the response of current with light intensity. The value of α has been accounted from the linear fit of log- log curve as 0.74. The non-unity value ($0.5 < \alpha < 1$) of α indicates that photo-responsivity of CsPbBr₃ may be attributed by combined effect of electron-hole pair generation, trapping within material and recombination. When light with high energy compared to band gap (E_g) incidents on the material, photons are absorbed by the material. As a consequences of which electron-hole pairs are generated ($h \rightarrow e^-+h^+$) within semiconducting CsPbBr₃. The photo generated electron-hole pairs are the prime essence of this phenomenon which enhance the conductivity of this material and decrease the potential barrier at the same time. Significant number of photo-generated holes recombine with Br-trapped electron. Therefore, unpaired electrons becomes the major charge carrier within material which are mainly contributing to the photo-physical properties.

Conclusion

CsPbBr₃ exhibits excellent dielectric and optoelectronic properties, making it a highly promising material for photodetector and semiconductor applications. The structural and morphological investigations confirmed the successful synthesis of well-crystallized CsPbBr₃ with predominantly cubic morphology. Electrical studies revealed a strong dependence of dielectric and conductivity parameters on temperature, indicating the thermally activated nature of charge transport within the material. Furthermore, the material demonstrated significant photoresponse under light illumination, with high photodetection efficiency and stable electrical behavior. These characteristics suggest effective generation,

separation, and transport of photogenerated charge carriers. The combination of favorable electrical properties, good crystallinity, and enhanced photoresponse highlights the potential of CsPbBr₃ for use in next-generation optoelectronic devices, including photodetectors, light-sensing systems, and semiconductor-based electronic components. Further optimization of synthesis conditions and device fabrication may lead to improved performance and broader practical applications.

Funding

No funding received for this work.

Acknowledgment

The authors express their gratitude to the Department of Chemistry Sheth M. N. Science College, Patan, and Department of Chemistry Amity University, Gwalior for their assistance with experimental work and analysis support.

References

1. Pious JK, Lekshmi ML, Muthu C, Rakhi RB, Nair VC. Zero-Dimensional Methylammonium Bismuth Iodide-Based Lead- Free Perovskite Capacitor. *ACS Omega*, 2017, 5798-5802. doi:10.1021/acsomega.7b00973
2. Park B, Philippe B, Zhang X, Rensmo H, Boschloo G, Johansson EMJ. Bismuth Based Hybrid Perovskites A₃Bi₂I₉ (A: Methylammonium or Cesium) for Solar Cell Application. *Adv mater*, 2015, 27, 6806-6813. doi:10.1002/adma.201501978
3. Dimesso L, Das C, Stöhr M, Jaegermann W. Investigation of cesium tin/leadiodide (CsSn_{1-x}Pb_xI₃) systems. *Mater Res Bull*. 2017, 85, 80-89. doi:10.1016/j.materresbull.2016.08.052
4. McClure ET, BallMR, WindlW, etal. Lead-freehalideperovskitesemiconductors Cs₂AgBiX₆ (X = Br , Cl) — New visible light absorbing , lead-free halide perovskite semiconductors. *Chem Mater*, 2016, 28(5), 1348-1354. doi:10.1021/acs.chemmater.5b04231
5. Li Z, YangM, ParkJS, WeiSH, BerryJJ, ZhuK. Stabilizing Perovskite Structures by Tuning Tolerance Factor: Formation of Formamidinium and Cesium Lead Iodide Solid-State Alloys. *Chem Mater*. 2016, 28(1), 284-292. doi:10.1021/acs.chemmater.5b04107
6. Ortega N, Kumar A, Bhattacharya P, Majumder SB, Katiyar RS. Impedance spectroscopy of multiferroic PbZr_xTi_{1-x}O₃/CoFe₂O₄ layered thin films. *Phys Rev B*. 2008, 77(1), 014111. doi:10.1103/PhysRevB.77.014111
7. James AR, Priya S, Uchino K, Srinivas K. Dielectric spectroscopy of Pb(Mg_{1/3}Nb_{2/3})O₃-PbTiO₃ single crystals. *J Appl Phys*. 2001, 90(7), 3504-3508. doi:10.1063/1.1401802
8. Feldman Y, Puzenko A, Ryabov Y. Dielectric relaxation phenomena in complex materials. *Adv Chem Phys*. 2006, 133, 125. doi:10.1002/0471790265.ch1
9. Dyre JC. Some remarks on ac conduction in disordered solids. *J Non Cryst Solids*. 1991, 135(2-3), 219-226. doi:10.1016/0022-3093(91)90423-4
10. Nowick A, Vaysleyb A, Kuskovsky I. Universal dielectric response of variously doped ionically conducting ceramics. *Phys Rev B - Condens Matter Mater Phys*. 1998, 58(13), 8398-8406. doi:10.1103/PhysRevB.58.8398
11. EL-MALLAH HM. AC Electrical Conductivity and Dielectric Properties of Perovskite (Pb , Ca) TiO₃ Ceramic. *Acta Phys Pol a*. 2012, 122(1), 174-179.
12. Anantharaman MR, Malini KA, Sindhu S, et al. Tailoring magnetic and dielectric properties of rubber ferrite composites containing mixed ferrites. *Bull Mater Sci*. 2001, 24(6), 623, doi:10.1007/BF02704011.
13. Ray A, Roy A, De S, Chatterjee S, Das S. Frequency and temperature dependent dielectric properties of TiO₂-V₂O₅ nanocomposites. *J Appl Phys*. 2018, 123(10), 104102. doi:10.1063/1.5012586.
14. Ullah A, Ullah A, Woo WS, Ahn CW, Kim IW. Dielectric spectroscopy of lead-free Bi_{0.5}(Na_{0.75}K_{0.25})_{0.5}TiO₃-BiAlO₃ ceramics. *Ceram Int*. 2014, 40, 11335-11342. doi:10.1016/j.ceramint.2014.03.116
15. Ray A, Roy A, Bhattacharjee S, et al. Correlation between the dielectric and electrochemical properties of TiO₂-V₂O₅ nanocomposite for energy storage application. *Electrochim Acta*. 2018, 291, 404-413, doi:10.1016/j.electacta.2018.02.033
16. Park W, Jo G, Hong W, et al. High-performance UV detector made of ultra-long ZnO bridging nanowires. *Nanotechnology*, 2009, 20, 45501, doi:10.1088/0957-4484/20/4/045501
17. Kaur R, Sharma V, Kumar M, Singh M, Singh A. Conductivity relaxation in Pb_{0.9}Sm_{0.1}Zr_{0.4}Ti_{0.495}Fe_{0.1}O₃ solid solution. *J Alloys Compd*. 2017, 735, 1472, doi:10.1016/j.jallcom.2017.11.254
18. Mohanty S, Choudhary RNP, Padhee R, Parida BN. Dielectric and impedance spectroscopy of BiFeO₃-NaTaO₃ multiferroics. *Ceramics International*. 2014, 40, 9017-9025.

19. Sheikh MS, Sakhya AP, Sadhukhan P, Dutta A, Das S, Sinha TP. Dielectric relaxation and Ac conductivity of perovskites $\text{CH}_3\text{NH}_3\text{PbX}_3$ (X = Br, I). *Ferroelectrics*. 2017, 514(1), 146-157. doi:10.1080/00150193.2017.1359023
20. Sheikh MS, Sakhya AP, Dutta A, Sinha TP. Dielectric relaxation of $\text{CH}_3\text{NH}_3\text{PbI}_3$ thin film. *Thin Solid Films*. 2017, 638, 277-281. doi:10.1016/j.tsf.2017.07.070
21. Song J, Li J, Li X, Xu L, Dong Y, Zeng H. Quantum Dot Light-Emitting Diodes Based on Inorganic Perovskite Cesium Lead Halides (CsPbX_3). *Adv Mater*. 2015, 27(44), 7162-7167. doi:10.1002/adma.201502567
22. Palazon F, Akkerman QA, Prato M, Manna L. X-ray lithography on perovskite nanocrystals films: From patterning with anion-exchange reactions to enhanced stability in air and water. *ACS Nano*. 2016, 10(1), 1224-1230. doi:10.1021/acsnano.5b06536
23. Wang Y, Li X, Song J, Xiao L, Zeng H, Sun H. All-Inorganic Colloidal Perovskite Quantum Dots: A New Class of Lasing Materials with Favorable Characteristics. *Adv. mater*, 2015, 27(44), 7101-7108. doi:10.1002/adma.201503573
24. Yakunin S, Protesescu L, Krieg F, et al. Low-threshold amplified spontaneous emission and lasing from colloidal nanocrystals of caesium lead halide perovskites. *Nat Commun*. 2015, 6, 1-8. doi:10.1038/ncomms9056
25. Lasing N, Xing G, Kumar MH, et al. Solution-Processed Tin-Based Perovskite for near-infrared lasing. *Adv. mater*, 2016, 28(37), 8191-8196. doi:10.1002/adma.20160141